analytical chemistry

ARTICLE

pubs.acs.org/ac

Magnetic Nanoparticle-Enhanced Biosensor Based on Grating-Coupled Surface Plasmon Resonance

Yi Wang, Jakub Dostalek,* and Wolfgang Knoll

Health & Environment Department, AIT Austrian Institute of Technology, Muthgasse 11/2, 1190 Vienna, Austria

Supporting Information

ABSTRACT: A highly sensitive surface plasmon resonance (SPR) biosensor employing magnetic nanoparticle (MNP) assays is presented. In the reported approach, MNPs simultaneously served as "vehicles" for rapid delivery of target analyte from a sample to the sensor surface and as labels increasing the measured refractive index changes that are associated with the binding of target analyte. An optical setup based on grating-coupled surface plasmon resonance (GC-SPR) was used with a magnetic field gradient applied through the sensor chip for manipulating with MNPs on its surface. Iron oxide MNPs and a sensor surface with metallic diffraction grating were modified with antibodies that specifically recognize different epitopes of the analyte of interest. The sensitivity of the biosensor was investigated as a function of mass transport of the analyte to the sensor surface driven by diffusion (free analyte) or by the magnetic field gradient (analyte bound to MNPs). Immunoassay-based detection of β human chorionic gonadotropin (βhCG) was implemented to evaluate the sensitivity of the MNP-enhanced GC-SPR biosensor scheme. The results reveal that the sensitivity of βhCG detection was improved by 4 orders of magnitude compared with the regular SPR sensor with direct detection format, and a limit of detection below pM was achieved.

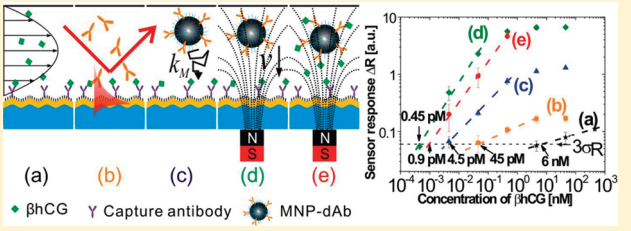

Surface plasmon resonance (SPR) biosensors are intensively researched for fast and sensitive detection of chemical and biological analytes in important fields such as medical diagnostics, food control, and environmental monitoring.[1−3] This optical method is based on the measurement of refractive index changes that are associated with the capture of target analyte on the metallic sensor surface by attached biomolecular recognition elements. SPR biosensors offer the advantage of direct and rapid analysis and typically allow detection of large and medium-size molecules at above nanomolar concentrations. To enhance the sensitivity, the amplifying of SPR biosensor response to molecular binding events was pursued on the basis of enzyme[4,5] and nanoparticle[6−10] labels. Gold nanoparticles were shown to strongly enhance the refractive index changes[11] which, for instance, allowed decreasing the limit of detection (LOD) for DNA strands to the femtomolar level.[9]

Similarly, magnetic nanoparticle (MNP) labels were employed in SPR biosensors[8,12,13] to increase the binding-induced refractive index changes[14] and in this[14] and other analytical techniques[15−22] allowed efficient preconcentration and purification of target analytes such as DNA,[22] RNA,[23] proteins,[24,25] cells,[21] bacteria,[26] and viruses[27] contained in complex samples. Moreover, in various optical biosensors MNPs were employed for the quick delivery of analyte to the sensor surface by magnetic field gradient, which allows overcoming a slow diffusion-driven mass transfer.[15,28−30] However, to our knowledge, this functionality has not to date been utilized for SPR biosensors. One of the reasons is that SPR biosensors mostly rely on the attenuated total reflection method (ATR) with Kretschmann configuration that is implemented by using bulk prism couplers and thus does not allow applying a magnetic field through the sensor chip.

In this paper, we report a new approach that combines SPR biosensor technology with MNP assays for detection and manipulating molecular analytes on the sensor surface. It is based on grating-coupled surface plasmon resonance (GC-SPR) with a metallic diffraction grating sensor chip that is functionalized by antibodies recognizing the target analyte. The MNPs conjugated with antibodies specific to different analyte epitopes served both as labels for enhancing refractive index changes due to the capture of target analyte and as "vehicles" for the rapid delivery of analyte from a sample solution to the sensor surface. They were rapidly collected on the sensor surface by magnetic field gradient applied directly through the GC-SPR sensor chip. The contribution of the velocity of MNPs in a magnetic field gradient to the sensitivity of MNP-enhanced GC-SPR biosensor is discussed, and its performance is demonstrated in an immunoassay experiment in which β human chorionic gonadotropin (βhCG) was detected.

MATERIALS AND METHODS

Materials. Magnetic nanoparticles (fluidMAG-ARA) with iron oxide core (magnetization saturation M_{sat} of 50 emu g^{-1} characterized by SQUID measurement), polysaccharide capping

Received: March 24, 2011
Accepted: June 28, 2011
Published: June 28, 2011

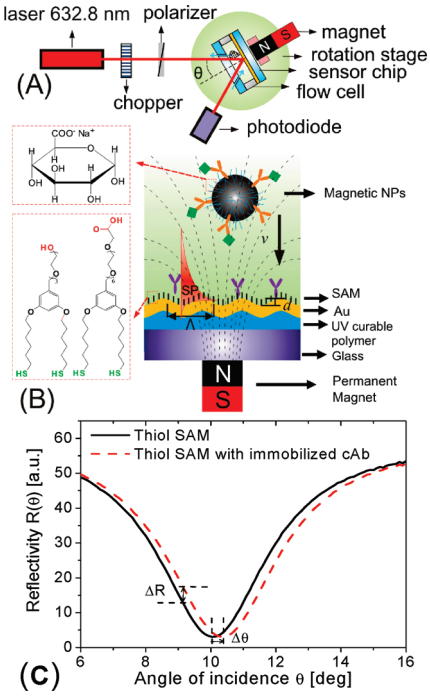

Figure 1. (A) Scheme of an optical setup and (B) a sensor chip of MNPs-enhanced GC-SPR sensor. (C) The angular SPR reflectivity spectra from a gold diffraction grating before and after the immobilization of capture antibody.

layer (thickness ~ 12.5 nm) were purchased from Chemicell (Berlin, Germany). The hydrodynamic diameter of magnetic nanoparticles of $d = 220 \pm 63$ nm was measured by dynamic light scattering (DLS, from Malvern Instruments, UK). A pair of capture (cAb, MAF05-627) and detection (dAb, MAF05-043) monoclonal antibodies that recognize different epitopes of β human chorionic gonadotropin (βhCG, A81455M) was obtained from Meridian Life Science (Saco, ME, USA). The affinity constant of the cAb was $K_A = 4 \times 10^{10}$ M^{-1} according to the manufacturer specification. 1-Ethyl-3-(3-dimethylaminopropyl)-carbodiimide (EDC) and *N*-hydroxysuccinimide (NHS) were from Pierce (Rockford, IL, USA). Dithiolalkanearomatic PEG6-COOH (thiol-COOH) and dithiolalkanearomatic PEG3-OH (thiol-PEG) were purchased from SensoPath Technologies (Bozeman, MT, USA). 2-(*N*-Morpholino)ethanesulfonic acid (MES), PBS buffer tablets, and Tween-20 were purchased from Sigma-Aldrich. PBS-Tween buffer (PBST) was prepared by adding Tween 20 (0.05%) in PBS buffer solution.

Optical Setup. An SPR biosensor setup depicted in Figure 1A was used. A light beam with a wavelength of $\lambda = 632.8$ nm was emitted from a He−Ne laser (Uniphase, CA, USA), passed through a chopper and a polarizer selecting transversal magnetic (TM) polarization, and was made incident at a surface of a sensor chip with gold diffraction grating. The sensor chip was mounted on a rotation stage (Huber AG, Germany) to control the angle of incidence, θ. The intensity of the laser beam that was reflected from the sensor chip surface was measured by using a photodiode (PD) connected to a lock-in amplifier (Princeton Applied Research, TN, USA). Against the surface of the sensor chip, a flow-cell with depth $h = 0.3$ mm, width $w = 4$ mm, and length $L = 8$ mm was attached. Samples were laminar-flowed over the sensor surface at a flow rate of 503 μL min^{-1}, which corresponds to the maximum flow velocity $v_{max} = 8.4$ mm s^{-1} at the distance from the surface $h/2$. For the MNP immunoassays, an external magnetic field with a gradient perpendicular to the surface of $\nabla B = 0.10$ T mm^{-1} was applied by using a 1.4 T NdFeB cylindrical magnet (diameter 10 mm, length 25 mm from Neotexx, Berlin, Germany) placed at a distance of 2 mm from the sensor surface. As seen in Figure 1C, the resonant coupling to surface plasmons by using diffraction grating coupler[1,31,32] is manifested as a resonance dip in the reflectivity spectrum $R(\theta)$. Similarly to SPR biosensors utilizing the ATR method, the binding of molecules to the gold surface is observed as a shift in the reflectivity dip, $\Delta\theta$. For the measurement of kinetics of reactions occurring on the surface, the angle of incidence was fixed at $\theta = 9°$, and the temporal binding-induced variations of reflectivity signal, $R(t)$, were recorded by using the software Wasplas (developed at the Max Plank Institute for Polymer Research, Mainz, Germany).

Sensor Chip Preparation. Silicon master grating with sinusoidal relief modulation (period $\Lambda = 520$ nm, depth = 58−64 nm) was prepared by using a holography and reactive ion beam etching (RIBE) as described previously.[33] The profile of the master grating was cast to a PDMS that was poured over its surface and cured overnight at 65 °C. Afterward, the PDMS stamp was detached, and the grating structure was transferred into a thin layer of UV-curable polymer (NOA72, Netherlands) deposited on a glass sensor chip surface by spin-coating. After 90 min exposure to UV light (4.8 mW cm^{-2} at a wavelength of $\lambda = 365$ nm, Bio-Link 365 from Vilber Lourmat, Germany), the PDMS stamp was released, and cured NOA72 polymer was aged for 9 h at 65 °C, then the sensor chip was coated with a thin gold layer (thickness of 60 nm) by sputtering (UNIVEX 450C from Leybold Systems, Germany). A thiol self-assembled monolayer (SAM) was formed on the gold surface (see Figure 1B) by overnight incubating in a mixture of thiol-COOH and thiol-PEG dissolved in absolute ethanol (molar ratio of 1:9 with a total concentration of 1 mM) followed by extensive rinsing with ethanol and drying in a stream of N_2.

The capture antibody cAb was in situ immobilized on the sensor surface by using amine coupling chemistry. First, the solution with EDC and NHS (concentrations in deionized water of 37.5 and 10.5 mg mL^{-1}, respectively)[34] was flowed over the surface for 10−15 min to convert the thiol SAM carboxylic moieties to active esters. Afterward, cAb dissolved in acetate buffer (10 mM, pH = 5.5) at a concentration of 30 μg mL^{-1} was circulated through the flow cell for 90 min to react via their amine groups with the sensor surface. Finally, the sensor surface was rinsed with PBS to remove loosely bound molecules. The reflectivity spectra $R(\theta)$ measured before the immobilization of cAb and after the rinsing are presented in Figure 1C. The measured resonance angle shift ($\Delta\theta = 0.35°$) corresponds to the surface coverage of antibody $\beta = 1.75$ ng mm^{-2} (0.012 pmol mm^{-2} for molecular weight of IgG antibodies of 150 kDa).

Modification of Magnetic Nanoparticles. MNPs were modified with detection antibody dAb according to the protocol from the supplier with several modifications. Briefly, 20 mg of MNPs was reacted with freshly prepared EDC and NHS (both concentrations of EDC and NHS of 11 mg mL^{-1} in MES buffer) to activate the carboxylic moieties on the MNP surface (see Figure 1B). Afterward, the MNPs were washed with pure MES buffer and incubated with 100 μg of dAb for 2 h at room temperature. Then the unreacted active ester groups on MNPs with covalently bound detection antibodies (MNP-dAb) were deactivated by 20-min incubation with 1 M ethanolamine

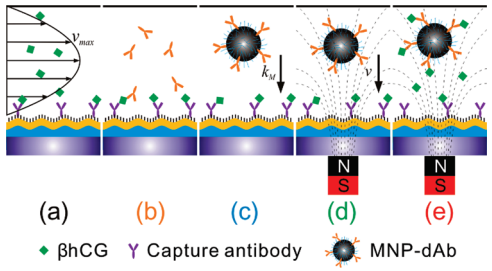

Figure 2. Schematics of used detection formats: direct detection (a), sandwich assays with amplification by detection antibody (b) and MNP-dAb without (c) and with (d) applied magnetic field. Detection format consisting of preincubating MNP-dAb with βhCG followed by sandwich assay upon applied magnetic field gradient (e).

(pH 8.5), followed by rinsing with PBST buffer. Prior to use, the modified nanoparticles were dissolved in PBST buffer at a concentration of 20 mg mL^{-1} and stored at 4 °C. The antibody-to-MNP ratio was estimated as 10:1, assuming 90% of antibodies were immobilized on the MNP surface during the labeling process.[35]

Detection Formats. All samples were prepared by spiking 0.8 mL of PBST with βhCG at concentrations ranging from 0.5 pM to 0.5 μM. As illustrated in Figure 2, five different detection formats (a−e) were evaluated for detection of the target analyte. In direct detection format a, PBST was flowed through the flow cell until a stable baseline in the SPR reflectivity signal, $R(t)$, was reached. Afterward, a sample was circulated through the sensor for 15 min, followed by 3-min rinsing with PBST. The sensor response was determined as a difference, ΔR, between the baseline and the reflectivity signal measured after the rinsing. In detection formats b−d, the sensor surface was subsequently incubated with 67 nM of dAb (detection format b) or with 0.6 nM of MNP-dAb (detection formats c and d) and rinsed with PBST for 5 min. In detection formats c and d, the magnetic field gradient was $\nabla B = 0$ and $\nabla B = 0.10$ T mm^{-1}, respectively, upon the 10-min incubation of the sensor surface with MNP-dAb. In detection format e, a sample was mixed with MNP-dAb at a concentration of 0.6 nM, allowed to react with βhCG for 20 min, and flowed through the flow cell with an applied magnetic field gradient of ∇B = 0.10 T mm^{-1} for 10 min. Afterward, the magnetic field was switched off ($\nabla B = 0$), and the sensor surface was rinsed for 5 min with PBST to wash MNP-dAb that was not affinity-bound to βhCG. The sensor response for detection formats b−e was determined as a reflectivity change, ΔR, before the sample injection and after the 5-min rinsing with PBST. Deionized water and 10 mM NaOH were sequentially flowed for around 10 min to release βhCG molecules bound to cAb on the surface (regeneration).

Mass Transfer of Analyte and MNP-dAb to the Surface. On the basis of the two-compartment model,[36] diffusion-driven mass transfer of βhCG and MNP-dAb from a sample in the flow-cell to the sensor surface can be described by the diffusion rate,

$$k_M \approx 1.378 \left(\frac{v_{max} D^2}{hL} \right)^{1/3} \quad (1)$$

where D is a diffusion constant in water. For βhCG and MNP-dAb, it was determined as $D = 1.1 \times 10^{-4}$ and 2×10^{-6} mm^2 s^{-1} from their hydrodynamic diameters d = 4 and 220 nm, respectively, based on the Stokes formula. Upon the drag of MNP-dAb

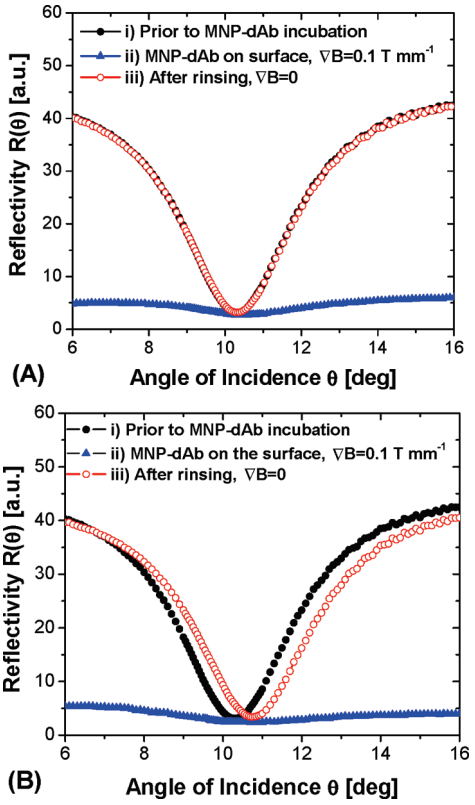

Figure 3. Specificity test of the sensor chip and MNP-dAb biointerface architectures. Angular reflectivity spectra measured in PBST (i) after 10-min flow of MNP-dAb with magnetic field gradient of $\nabla B = 0.1$ T mm^{-1} (ii), and after switching off the magnetic field and 2-min rinsing with PBST (iii). The results are shown for sensor surface without (A) and with (B) the flow of a sample with 45 nM βhCG prior to the experiment.

through the aqueous sample with a dynamic viscosity of μ = 1 g m^{-1} s^{-1} by an applied magnetic field gradient, ∇B, its steady state velocity, v, can be determined from the following equation,

$$v = d^2 \rho M_{sat} \nabla B / 18\mu \quad (2)$$

where $\rho = 5$ g cm^{-3} is the bulk density of iron oxide MNPs, M_{sat} is the saturation magnetization, and d is the hydrodynamic diameter of MNP-dAb. For the hCG, the diffusion rate is equal to $k_M = 4.8 \times 10^{-3}$ mm s^{-1}, which is larger than the one for MNPs $k_M = 3.3 \times 10^{-4}$ mm s^{-1}, owing to its smaller size. The predicted steady state velocity of MNPs dragged through an aqueous sample by the applied magnetic field gradient of $\nabla B = 0.10$ T mm^{-1} is equal to $v = 6 \times 10^{-2}$ mm s^{-1}, which is ~13- and 180-fold faster than diffusion rates for hCG and MNP, respectively. For the investigated βhCG SPR biosensor, the binding kinetics was diffusion-controlled, as the affinity binding rate multiplied by the cAb surface coverage $k_a\beta \sim 1.2 \times 10^{-2}$ mm s^{-1} was larger than k_M (the affinity rate constant of $k_a \sim 10^6$ M^{-1} s^{-1} was determined for the interaction between cAb and βhCG by SPR measurement; data not shown). These data indicate that magnetic nanoparticle assay can provide faster delivery of the analyte to the surface and thus provide enhanced SPR sensor response.

RESULTS AND DISCUSSION

Sensor Specificity. First, a control experiment was performed in which a blank sample without the target βhCG analyte was

dx.doi.org/10.1021/ac200751s |Anal. Chem. 2011, 83, 6202–6207

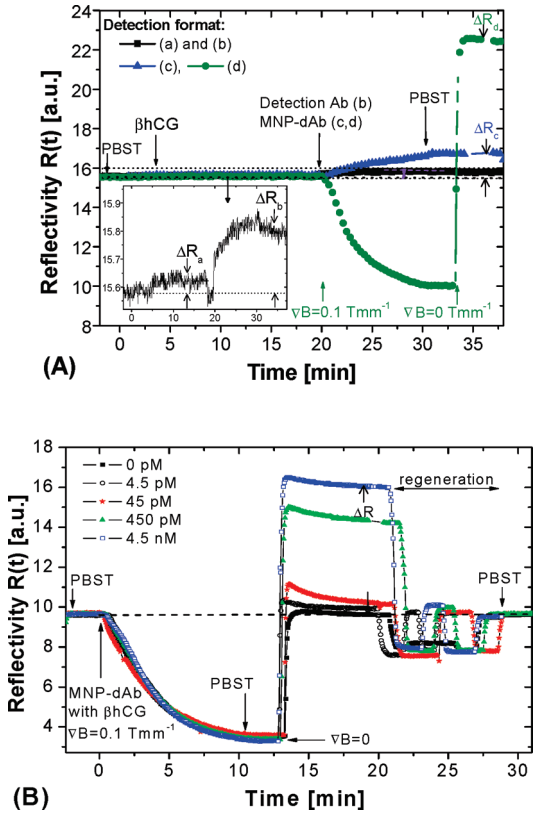

Figure 4. (A) Comparison of the reflectivity signal, $R(t)$, measured for a βhCG concentration of 4.5 nM and direct detection format (a, squares and the inset), antibody amplification (b, squares and the inset), MNP-dAb amplification (c, triangles), MNP-dAb amplification with magnetic field gradient ∇B = 0.10 T mm^{-1} (d, circles). (B) Reflectivity signal, $R(t)$, for the detection of βhCG at concentrations between 0 and 4.5 nM by using detection format e.

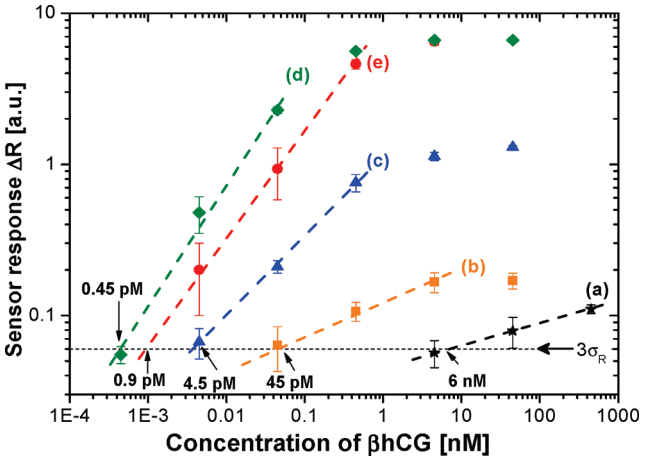

Figure 5. The calibration curves for the detection of βhCG by direct detection format (a, stars), followed by antibody amplification (b, squares) and the amplification by MNP-dAb without (c, triangles) and with (d, diamonds) an external magnetic field. In format e, a sample with βhCG was incubated with MNP-dAb, followed by the detection of the MNP-dAb-βhCG complexes with external magnetic field applied (circles).

analyzed by using the detection format d. Figure 3A shows the angular reflectivity spectra, $R(\theta)$, measured before the incubation with MNP-dAb (i) and after a 10-min flow of MNP-dAb with magnetic field gradient ∇B = 0.10 T mm^{-1} (ii) that was followed by the rinsing with PBST with the magnetic field switched off (iii). These results show that the overall reflectivity decreased upon the collecting of MNP-dAb on the sensor surface in the magnetic field gradient due to the aggregation of MNPs and accompanied scattering of incident laser beam (curve ii). However, the reflected laser beam intensity and resonance angle of the SPR dip reached the original levels after the rinsing (curve iii), which indicates negligible nonspecific interaction between MNP-dAb and the sensor surface functionalized with cAb. For comparison, Figure 3B shows an identical experiment for a sample with βhCG at 45 nM concentration. The angular reflectivity spectra, $R(\theta)$, before the injecting of MNP-dAb (i) and after the rinsing (iii) reveal a clear shift in the resonance angle ($\Delta\theta$ = 0.45°), which is attributed to the specific binding of MNP-dAb to βhCG captured by cAb on the surface of the sensor chip.

MNP-Amplified Sensor Response. The MNP amplification of GC-SPR sensor response was studied for the concentration of βhCG set to 4.5 nM. Figure 4A shows the kinetics of the SPR reflectivity signal $R(t)$ upon sample analysis with detection formats a, b, c, and d. For direct detection format a, a small reflectivity change of ΔR_a = 0.06 ± 0.017 was observed,. as seen in the inset of Figure 4A. The binding of the detection antibody (format b) led to an ~3-fold increased reflectivity change, ΔR_b = 0.2 ± 0.017 with respect to direct detection format a. Because the kinetics for the binding of detection antibody saturated after the 10-min incubation, we assumed that the majority of accessible βhCG molecules captured on the sensor surface reacted with detection antibodies. The 3-fold increase, $\Delta R_b/\Delta R_a$, of the sensor response is lower than the ratio of the molecular weights of the antibody (150 kDa) and βhCG (22.2 kDa). This fact is probably caused by steric hindrance, leading to only ~30% of βhCG molecules being accessible for the binding of the dAb.

For the MNP-enhanced sandwich assay with diffusion-driven mass transfer of MNP-dAb to the surface (detection format c), a sensor response of ΔR_c = 1.02 ± 0.015 was observed, which is ~17 times higher than that for format a. This enhancement is due to the larger mass and higher refractive index of the MNPs. Let us note that the sensor response was not saturated after the 10 min flow of MNP-dAb. If a magnetic field gradient is applied upon the flow of MNP-dAb (detection format d), one can see a gradual decrease in the reflectivity signal, $R(t)$, owing to the accumulation of nanoparticles on the surface and the associated scattering. However, upon rinsing, the reflectivity signal rapidly increased, and a large sensor response of ΔR_d = 6.4 ± 0.021 was measured. This reflectivity change is ~10^2 times larger than that for the direct detection (detection format a) and 6.3 fold higher than for MNP-dAb diffusing to the surface (detection format c). This observation can be explained by the rapid magnetically driven mass transfer of MNP-dAb ($v = 6 \times 10^{-2}$ mm s^{-1}), which is ~1.8×10^2 times faster than the mass transfer of MNP-dAb driven by diffusion ($k_M = 3.3 \times 10^{-4}$ mm s^{-1}). The sensor response enhancement $\Delta R_d/\Delta R_c$ is lower than the ratio of the mass transfer rates v/k_M because the sensor response does not change linearly in time for detection format d and gets quickly saturated (see curve d in Figure 4A).

Figure 4B compares the SPR reflectivity signal, $R(t)$, measured by using detection format e for analyte concentrations between 0

dx.doi.org/10.1021/ac200751s |Anal. Chem. 2011, 83, 6202–6207

and 4.5 nM. Similar to the detection format d, $R(t)$ decreased after the injection of MNP-dAb with captured βhCG, and it rapidly increased after the removal of the magnet from the sensor surface and rinsing. The reflectivity change, ΔR_e, after rinsing increases with the concentration of βhCG in the sample that was reacted with MNP-dAb. In addition, Figure 4B illustrates that the sensor surface can be regenerated after detection, which allowed more than 15 detection cycles with one sensor chip (Figure S1 of the Supporting Information).

Limit of Detection (LOD). The calibration curves for the detection of βhCG by using detection formats a−e are plotted in Figure 5 for concentrations between 0.45 pM and 45 nM. For each concentration and detection format, the sensor response, ΔR, was measured in triplicate, and the error bar was calculated. The calibration curve for direct detection (format a) indicates that the sensor response was close to saturation at concentrations above nanomolar because the slope in the log−log scale was significantly lower than 1. This can be explained by the high affinity constant, $K_A \sim 4 \times 10^{10}$ M^{-1}, of the capture antibody. Similarly, the slope for the dAb and MNP-dAb amplification calibration curves b−d is lower than 1, and above nanomolar concentration, the response saturates. The calibration curve for detection format e approaches its maximum at βhCG concentrations above 1 nM, which corresponds to the saturation of dAb binding sites that are carried by MNP-dAb mixed with the analyte. The sensor response saturation for detection format c occurs at much lower levels than for formats d and e. The reason is the slow diffusion-limited mass transfer of MNP-dAb to the surface (detection format c) that leads to the fact that the binding of MNP-dAb did not reach equilibrium for any βhCG concentration.

The LOD was determined as the βhCG concentration at which the sensor response, ΔR, was equal to 3 times the standard deviation of the baseline reflectivity noise, $3\sigma_R = 0.06$. The LOD for the direct detection (a) was 6 nM. Through the amplification by detection antibody binding (b), the LOD was improved by ∼2 orders of magnitude to 45 pM. With MNP amplification (c), the LOD was further decreased to 4.5 pM, which is around 3 orders of magnitude lower than that for direct detection. The enhanced mass transfer of MNPs through the applied magnetic field (d) allowed reaching an even lower LOD of 0.45 pM: more than 4 orders of magnitude lower than by direct detection. For detection format e, a similar LOD, ∼0.9 pM, was observed for the detection of βhCG that was preincubated with MNP-dAb. The LOD for detection format e is about 2-fold higher than that for detection format d, which does not agree with the assumption that the sensor response can be increased by the enhancing of the mass transfer of βhCG ($k_M = 4.8 \times 10^{-3}$ mm s^{-1} for format d) through pulling MNPs by a magnetic field gradient ($\nu = 6 \times 10^{-2}$ mm s^{-1} for format e). This is probably due to the steric hindrance of the binding of βhCG decorated on MNPs to the surface with cAb; possible dissociation of the βhCG and MNP-dAb complexes; and the aggregation of MNP-dAb in the magnetic field, preventing the forming of a monolayer on the surface. Let us note that the lowest achieved LOD of 0.45 pM for detection format d is comparable with that demonstrated by a sensitive but more complex surface plasmon-enhanced fluorescence spectroscopy (0.6 pM)[37], and it is around 3 orders of magnitude better than that reported for a SPR biosensor with a sandwich assay (0.13 nM)[38] and SP-enhanced diffraction detection scheme (0.2 nM).[39]

CONCLUSIONS

We combined a grating-coupled surface plasmon resonance (GC-SPR) with magnetic nanoparticle (MNP) immunoassays for biosensor applications that require high sensitivity. The presented results demonstrate that this sensor scheme enables simple manipulating with molecular analytes on the sensor surface by using a magnetic field gradient that can be applied through a sensor chip. Particularly, it offers the advantage of enhancing refractive index changes associated with the analyte capture on the surface and allows increasing the slow diffusion-limited mass transfer from a sample to the sensor surface. The performance characteristics of this approach were evaluated by a series of experiments in which βhCG was detected by direct and sandwich immunoassay formats. The results show that the MNP-enhanced format using collecting the nanoparticles on the surface by a magnetic field improved the sensitivity by ∼4 orders of magnitude with respect to regular SPR utilizing a direct detection format. A limit of detection of 0.45 pM was achieved, which is comparable with the best reported results by other, more complex biosensor schemes relying on SPR. Future work will be devoted to the implementation of this detection principle for the analysis of large analytes, such as bacterial pathogens or viruses. Mass transfer to the surface is strongly hindered by diffusion for these analytes and, thus, impedes the sensitivity of SPR biosensor technology.

ASSOCIATED CONTENT

Supporting Information. A reflectivity kinetic figure that illustrates the sensor regeneration. This material is available free of charge via the Internet at http://pubs.acs.org.

AUTHOR INFORMATION

Corresponding Author

*Fax: +43(0) 50550-4450. E-mail: jakub.dostalek@ait.ac.at.

ACKNOWLEDGMENT

The authors acknowledge Raquel Chuliá Jordan from the Max Planck Institute for Polymer Research in Mainz (Germany) for preparation of the diffraction grating master by using holography and RIBE and Dr. Haitao Gao from Johannes Gutenberg University in Mainz (Germany) for the magnetization measurement with the SQUID magnetometer. Support for this work was provided in part by the Center of Innovation and Technology of Vienna (ZIT).

REFERENCES

(1) Knoll, W. *Annu. Rev. Phys. Chem.* **1998**, *49*, 569–638.
(2) Homola, J. *Chem. Rev.* **2008**, *108*, 462–493.
(3) Homola, J. *Anal. Bioanal. Chem.* **2003**, *377*, 528–539.
(4) Goodrich, T. T.; Lee, H. J.; Corn, R. M. *J. Am. Chem. Soc.* **2004**, *126*, 4086–4087.
(5) Lee, H. J.; Li, Y.; Wark, A. W.; Corn, R. M. *Anal. Chem.* **2005**, *77*, 5096–5100.
(6) He, L.; Musick, M. D.; Nicewarner, S. R.; Salinas, F. G.; Benkovic, S. J.; Natan, M. J.; Keating, C. D. *J. Am. Chem. Soc.* **2000**, *122*, 9071–9077.
(7) Lee, H. J.; Wark, A. W.; Corn, R. M. *Analyst* **2008**, *133*, 596–601.
(8) Mitchell, J. S.; Wu, Y. Q.; Cook, C. J.; Main, L. *Anal. Biochem.* **2005**, *343*, 125–135.

(9) Wark, A. W.; Lee, H. J.; Qavi, A. J.; Corn, R. M. *Anal. Chem.* **2007**, *79*, 6697–6701.
(10) Frasconi, M.; Tortolini, C.; Botre, F.; Mazzei, F. *Anal. Chem.* **2010**, *82*, 7335–7342.
(11) Fang, S. P.; Lee, H. J.; Wark, A. W.; Corn, R. M. *J. Am. Chem. Soc.* **2006**, *128*, 14044–14046.
(12) Wang, J. L.; Munir, A.; Zhu, Z. Z.; Zhou, H. S. *Anal. Chem.* **2010**, *82*, 6782–6789.
(13) Teramura, Y.; Arima, Y.; Iwata, H. *Anal. Biochem.* **2006**, *357*, 208–215.
(14) Soelberg, S. D.; Stevens, R. C.; Limaye, A. P.; Furlong, C. E. *Anal. Chem.* **2009**, *81*, 2357–2363.
(15) Tseng, P.; Di Carlo, D.; Judy, J. W. *Nano Lett.* **2009**, *9*, 3053–3059.
(16) Hsing, I. M.; Xu, Y.; Zhao, W. T. *Electroanalysis* **2007**, *19*, 755–768.
(17) Katz, E.; Weizmann, Y.; Willner, I. *J. Am. Chem. Soc.* **2005**, *127*, 9191–9200.
(18) Willner, I.; Katz, E. *Angew. Chem., Int. Ed.* **2003**, *42*, 4576–4588.
(19) Perez, J. M.; Josephson, L.; O'Loughlin, T.; Hogemann, D.; Weissleder, R. *Nat. Biotechnol.* **2002**, *20*, 816–820.
(20) Perez, J. M.; Simeone, F. J.; Tsourkas, A.; Josephson, L.; Weissleder, R. *Nano Lett.* **2004**, *4*, 119–122.
(21) Jun, B. H.; Noh, M. S.; Kim, J.; Kim, G.; Kang, H.; Kim, M. S.; Seo, Y. T.; Baek, J.; Kim, J. H.; Park, J.; Kim, S.; Kim, Y. K.; Hyeon, T.; Cho, M. H.; Jeong, D. H.; Lee, Y. S. *Small* **2010**, *6*, 119–125.
(22) Nam, J. M.; Thaxton, C. S.; Mirkin, C. A. *Science* **2003**, *301*, 1884–1886.
(23) Zhang, H. Y.; Lee, M. Y.; Hogg, M. G.; Dordick, J. S.; Sharfstein, S. T. *ACS Nano* **2010**, *4*, 4733–4743.
(24) Tsai, H. Y.; Chan, J. R.; Li, Y. C.; Cheng, F. C.; Fuh, C. B. *Biosens. Bioelectron.* **2010**, *25*, 2701–2705.
(25) Peyman, S. A.; Iles, A.; Pamme, N. *Lab Chip* **2009**, *9*, 3110–3117.
(26) Gu, H. W.; Ho, P. L.; Tsang, K. W. T.; Wang, L.; Xu, B. *J. Am. Chem. Soc.* **2003**, *125*, 15702–15703.
(27) Wang, G. N.; Gao, Y. A.; Huang, H.; Su, X. G. *Anal. Bioanal. Chem.* **2010**, *398*, 805–813.
(28) Bruls, D. M.; Evers, T. H.; Kahlman, J. A. H.; van Lankvelt, P. J. W.; Ovsyanko, M.; Pelssers, E. G. M.; Schleipen, J.; de Theije, F. K.; Verschuren, C. A.; van der Wijk, T.; van Zon, J. B. A.; Dittmer, W. U.; Immink, A. H. J.; Nieuwenhuis, J. H.; Prins, M. W. J. *Lab Chip* **2009**, *9*, 3504–3510.
(29) Dittmer, W. U.; Evers, T. H.; Hardeman, W. M.; Huijnen, W.; Kamps, R.; de Kievit, P.; Neijzen, J. H. M.; Nieuwenhuis, J. H.; Sijbers, M. J. J.; Dekkers, D. W. C.; Hefti, M. H.; Martens, M. *Clin. Chim. Acta* **2010**, *411*, 868–873.
(30) Liang, C. H.; Wang, C. C.; Lin, Y. C.; Chen, C. H.; Wong, C. H.; Wu, C. Y. *Anal. Chem.* **2009**, *81*, 7750–7756.
(31) Dostalek, J.; Homola, J. *Sens. Actuators, B* **2008**, *129*, 303–310.
(32) Homola, J.; Koudela, I.; Yee, S. S. *Sens. Actuators, B* **1999**, *54*, 16–24.
(33) Zhang, N.; Liu, H.; Knoll, W. *Biosens. Bioelectron.* **2009**, *24*, 1783–1787.
(34) Wang, Y.; Brunsen, A.; Jonas, U.; Dostalek, J.; Knoll, W. *Anal. Chem.* **2009**, *81*, 9625–9632.
(35) Koh, I.; Wang, X.; Varughese, B.; Isaacs, L.; Ehrman, S. H.; English, D. S. *J. Phys. Chem. B* **2006**, *110*, 1553–1558.
(36) Edwards, D. A.; Goldstein, B.; Cohen, D. S. *J. Math. Biol.* **1999**, *39*, 533–561.
(37) Vareiro, M. L. M.; Liu, J.; Knoll, W.; Zak, K.; Williams, D.; Jenkins, A. T. A. *Anal. Chem.* **2005**, *77*, 2426–2431.
(38) Boozer, C.; Yu, Q. M.; Chen, S. F.; Lee, C. Y.; Homola, J.; Yee, S. S.; Jiang, S. Y. *Sens. Actuators, B* **2003**, *90*, 22–30.
(39) Yu, F.; Knoll, W. *Anal. Chem.* **2004**, *76*, 1971–1975.